Dry-transfer technique for polymer-free single-walled carbon nanotube saturable absorber on a side polished fiber

ARAM A. MKRTCHYAN,[1,2] YURIY G. GLADUSH,[1,4] DIANA I. GALIAKHMETOVA,[1] VSEVOLOD YA. YAKOVLEV,[1] VADIM T. AHTYAMOV,[2] AND ALBERT G. NASIBULIN[1,3,*]

[1]*Skolkovo Institute of Science and Technology, Moscow, Russia*
[2]*Moscow Institute of Physics and Technology, Dolgoprudny, Moscow Region, Russia*
[3]*Aalto University, Espoo, Finland*
[4]*y.gladush@skoltech.ru*
*a.nasibulin@skoltech.ru

Abstract: We fabricate single-walled carbon nanotube saturable absorbers on a side-polished fiber by a dry transfer technique. We demonstrate that this method allows for the easy and robust implementation of polymer-free carbon nanotube film for an evanescent field interaction in the fiber laser cavity. The high-quality single-walled carbon nanotubes are synthesized by the aerosol CVD method with absorption maximum tuned to an erbium doped fiber laser emission line. The Q-switch and mode-lock regimes as well as the harmonic mode-lock regime with the 79th order are successfully demonstrated with this approach. Critical power for damage threshold is estimated.

1. Introduction

Since last decade pulse fiber lasers have proven to be a reliable source for many applications in medicine (eye surgery, cosmetology, dental treatment, *etc.*), optical tomography and spectroscopy, material processing (cutting, marking and engraving). Saturable absorbers (SAs) play a crucial role in the fiber lasers passive pulse generation. Nowadays, there is a number of novel materials like graphene [1,2], black phosphorus [3,4], topological insulators [5] and transition-metal dichalcogenides (MoS_2 [6], $MoSe_2$ [7]) that have been thoroughly investigated as an alternative of a standard SESAM for an ultrafast fiber optics. In parallel, carbon nanotubes have been widely explored and demonstrated good performance because of their excellent properties, such as wideband operation, fast recovery time, stability and low cost [8]. The first pulsed fiber laser based on a single-walled carbon nanotube (SWCNT) saturable absorber with mode-locked pulses was demonstrated in 2004 [9]. It is worth mentioning that 66 fs-long mode-lock pulse generation has been achieved with a carbon nanotube saturable absorber [10], which is close to the world record of 37 fs pulse generation in erbium-doped fiber lasers [11]. The most widely used approach implies SWCNT-SA in the form of a SWCNT-polymer composite. However, polymers might substantially decrease the stability of SWCNT-SA due to smaller thermal damage threshold of polymers compared to SWCNTs [12–14]. To avoid the SA degradation, a few approaches for a polymer-free SWCNT-SA fabrication were proposed: the spray method [15–17], the optical deposition method [17,18], vertically aligned SWCNT incorporation technique [19,20] and dry transfer technique [21,22]. The last one offers great advantages in terms of fabrication simplicity and reproducibility of SA parameters. This method was applied to deposit aerosol CVD synthesized SWCNTs on the fiber ferrule to work in the erbium [23] and bismuth [24] all-fiber laser schemes. In this case the laser power is limited to a few tens of mW determined by the damage threshold of the SWCNTs. To increase the laser output power it was proposed to

utilize SA on a side-polished or tapered fiber [10,19,20,25–31], so that only the evanescent tail of the light, propagating through the fiber, interacts with the SWCNTs. This method dramatically increases the limit of the output laser power up to hundreds of mW.

In the present paper, we implement for the first time aerosol CVD synthesized high-quality SWCNTs on a D-shape fiber for a polymer-free SA and demonstrate its capability to adjust the desired pulse generation regime. We apply the dry transfer technique for a sample fabrication and show that this method allows fast, easy and reproducible transfer of the saturable absorber material to the D-shape fiber surface. The diameter of SWCNTs and therefore their absorption peak is adjusted during the synthesis to the emission line of the erbium doped fiber laser. We characterize samples in terms of transmittance anisotropy and nonlinear optical transmittance. Finally, we implement SWCNT-SA in the fiber laser and demonstrate its capability to foster laser generation in Q-switch, mode-lock and harmonic mode-lock regimes.

2. Sample preparation technique

As a saturable absorber material, we synthesize SWCNTs by an aerosol CVD method described in detail elsewhere [32]. This method utilizes a spark discharge technique to generate iron nanoparticles, which are introduced in a nitrogen atmosphere in the reactor, mixed with a laminar flow of carbon monoxide (CO) and hydrogen (H_2) and heated up to $880\,°$ C. The SWCNTs grown in the reactor are collected downstream of the furnace on nitrocellulose filters. A mean diameter of SWCNTs can be easily tuned during the synthesis in the range from 1 to 2.3 nm by adding a certain concertation of CO_2 in the flow [33]. In our experiments we grow SWCNTs with a mean diameter of 1.4 nm, which corresponds to 1560 nm for S_{11} transition of semiconducting nanotubes close to the emitting wavelength of the erbium fiber laser. The optical spectrum of SWCNTs is measured with a photospectrometer Lambda 900 UV-Vis-NIR shown in Fig. 1(a). Raman measurements (Thermo Scientific DXRxi Raman Imaging Microscope) with a 532 nm laser revealed high ratio between intensities of G and D bands confirming high quality of the SWCNTs (Fig. 1(b)). The morphology of the SWCNTs studied with scanning electron microscope shows that the nanotubes form a randomly oriented film on the substrate surface (inset in Fig. 1(b)).
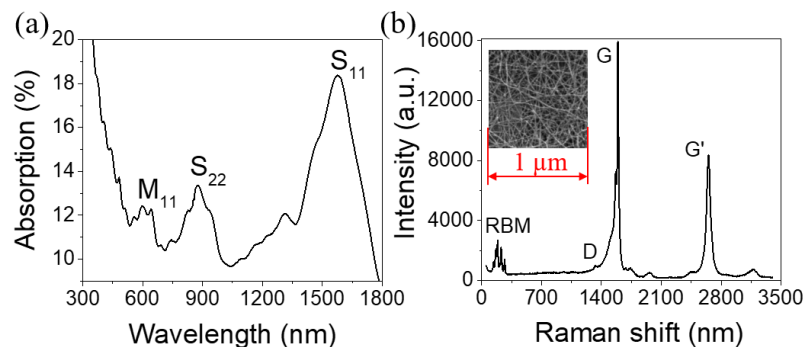

Fig. 1. (a) Spectrum of aerosol CVD grown SWCNTs, where S_{11} and S_{22} transitions correspond to semiconducting SWCNTs and M_{11} transition to metallic one. (b) Raman spectrum of the SWCNTs measured with a 532 nm laser. Inset: Scanning electron microscope image of the SWCNT film.

D-shape fibers are produced by Phoenix Photonics with a standard single-mode fiber (SMF28) with a 17 mm side-polished region. It correspondingly has insertion losses of 0.1 and 56 dB with air and index-matched oil with the refractive index of 1.5. To deposit SWCNTs from the filter onto the D-shape fiber we use the dry transfer technique: SWCNTs collected on the filter are simply transferred by pressing towards the D-shape fiber surface (Fig. 2). A weak adhesion of the SWCNT films to the nitrocellulose filter and strong

adhesion to the quartz ensures nanotubes stick to the D-shape fiber surface. The absorption of the saturable absorber can be controlled by the thickness and the length of the deposited SWCNT film.
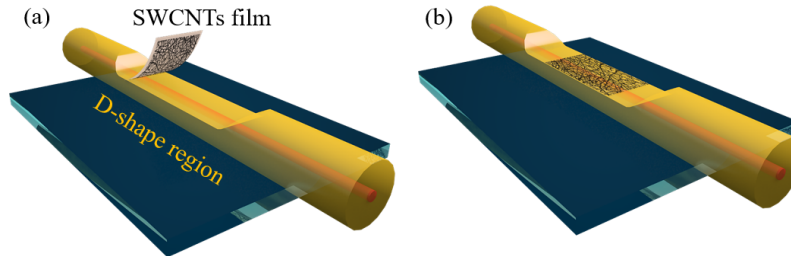

Fig. 2. Schematic view of the SWCNT deposition onto the D-shape fiber using the dry transfer technique: (a) a filter with the collected SWCNTs approaches and being pressed to the D-shape fiber, (b) SWCNTs deposited onto the D-shape fiber.

3. Characterization of the sample

Linear losses of the saturable absorber on the D-shape fiber have a large influence on pulse dynamics in the fiber laser. First of all, the evanescent field interaction geometry results in higher saturation intensity compared to the same material disposed on a fiber ferrule. To compensate this effect researchers usually utilize samples with a relatively high absorption, more than 6 dB [31,34,35]. Second, these losses are always polarization dependent giving rise to the nonlinear polarization evolution (NPE) mechanism and their contribution to the pulse shaping, considered to be unwanted fo our purposes. For the sample preparation we have taken the SWCNT film with 20 nm thickness and 4 mm length leading to 3.35 dB of the sample absorption in nonpolarized light given by erbium ASE source with the 1530-1580 spectral width. This relatively low absorption provides a compromise between the desired low nonsaturable losses and higher modulation depth of the saturable absorption on one hand and keeping polarization dependent losses (PDL) small on the other hand.

To measure PDL, we use experimental setup shown in Fig. 3(a), where erbium broadband ASE source is used for an input light. Here, we utilize an optical fiber-to-fiber U-bench, in which we add a rotating optical polarizer to control the polarization state of the light, propagating through the sample. 50% of the light propagates through the sample and the other 50% fraction is used as the reference. Results of the measurements (Fig. 4(a)) show that the PDL is equal to 1.28 dB. The sample absorbs 60.6% and 47.1% for out-of-plane (maximum transmittance) and in-plane (minimum transmittance) polarizations. As we discuss in the laser section, small PDL allows us to exclude NPE contribution to the pulse shaping mechanism in a mode-lock regime.

Next we measure nonlinear absorption for both in-plane and out-of-plane polarization of the laser. We use a commercially available mode-locked polarization maintaining pulsed fiber laser with a 6 ps pulse duration. Maximum mean power of the pulsed laser is 5 mW and maximum pulse energy is 508 pJ. The experimental setup is shown in Fig. 3(b). To probe with defined polarization, we use a commercial splicer with rotating fiber holders to bring together laser out fiber and the sample. This adds the additional losses reducing the input power to 2 mW. By rotating a fiber holder of the splicer we find the maximum transmittance (out-of-plane polarization) and minimum transmittances (in-plane polarization) in the linear regime, then after fixing the light polarization, we measure nonlinear transmittance by changing the light power with the attenuator. In this case instead of 50/50 coupler we used 1/99 coupler, in which 99% of the light goes through the sample.
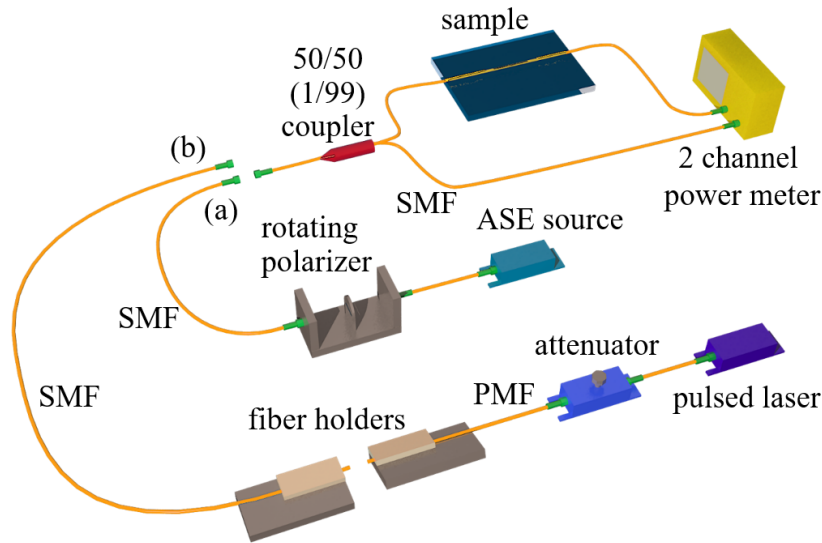
Fig. 3. Experimental setup for measurements of (a) the polarization depended losses (PDL) of the SWCNT-SA on a D-shape fiber with a rotating polarizer, (b) the sample nonlinear transmittance.
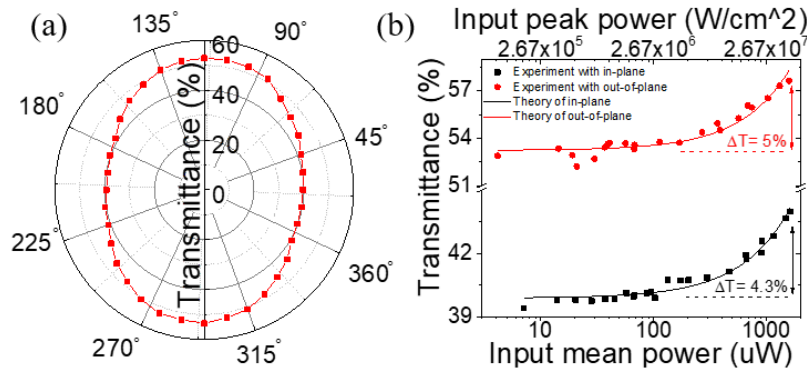

Fig. 4. Transmittance of the sample shown (a) in polar coordinates, which minimum and maximum values correspond to in-plane and out-of-plane polarizations, respectively; (b) versus the input power for the in-plane and out-of-plane polarizations.

With the lasers available power, we are able to reach the modulation depths of $\Delta T = 4.3\%$ for the in-plane and $\Delta T = 5\%$ for the out-of-plane polarization (Fig. 4(b)). However, as one can see we are far from reaching the saturation intensity and much higher modulation depth can be obtained for higher power or shorter pulses.

4. Pulsed laser with SWCNT-SA on the D-shape fiber

To test the saturable absorber, we implement it into the ring cavity fiber laser with relatively short resonator optimized for a stable laser generation. We use 1.4 meters highly doped erbium fiber having 45.9 ps^2 dispersion at 1555 nm (shown in Fig. 5). The laser is pumped by a diode laser at 980 nm with the maximum output power of 450 mW. It is followed by polarization insensitive isolator, polarization controller, a sample and 50/50 output coupler. The full length of the resonator is 7.65 m and net dispersion is -0.07 ps^2 (anomalous dispersion).

First of all, we observe a single-soliton mode-locked regime self-starting at 26.6 mW pump power and 1.18 mW output power. Figure 6 shows the autocorrelation trace, pulse

train and spectrum of the single soliton regime. Spectral full width at half maximum (FWHM) is found to be 7.4 nm, the pulse duration calculated from the sech^2 fit is 372 fs. The pulse energy and fundamental cavity repetition rate are correspondingly 44.3 pJ and 27 MHz. The time-bandwidth product is equal to 0.367, which is close to the theoretical limit of 0.315. It means that our pulses are almost transform limited and no further compression is possible. Radiofrequency spectrum is shown at Fig. 6(d-f) for fundamental repetition rate and 71st harmonics. On this frequency range the signal to noise ratio decreases only from 64 to 60 dB. With increasing of the pump power, the laser starts to generate pulses in the multi-soliton regime.
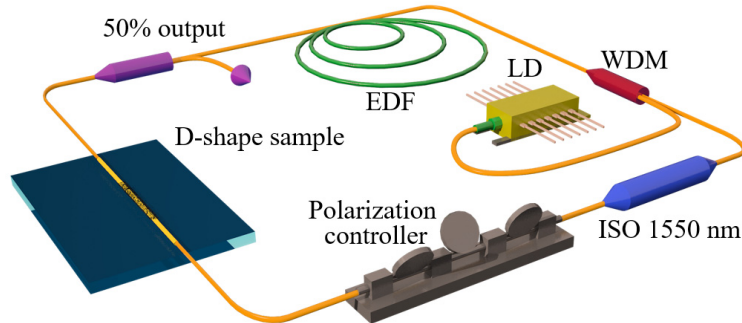

Fig. 5. All fiber laser scheme with a SWCNT-SA on the D-shape fiber in the ring resonator.
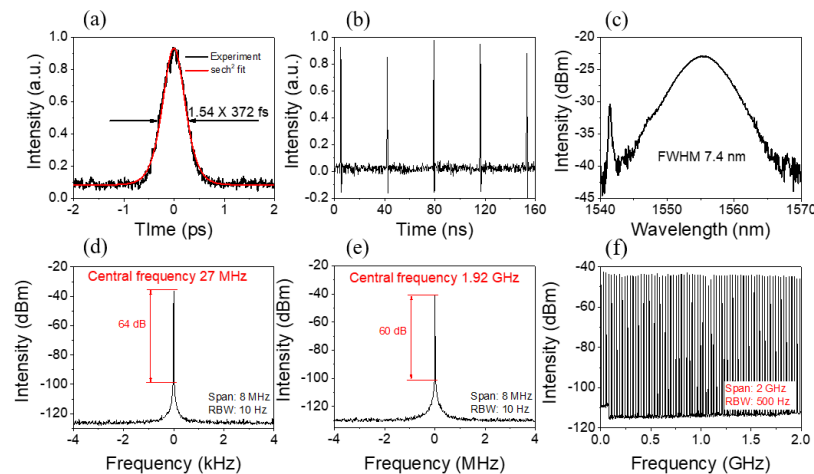

Fig. 6. Experimental results obtained for the single-soliton mode-lock pulse regime: (a) autocorrelation trace and its theoretical fit with the pulse width of 372 fs; (b) pulse train; (c) pulse spectrum with the full width at half maximum of 7.4 nm. Bottom panel represents radiofrequency spectrum at fundamental repetition rate (d), 71st harmonic (e) and wide span of 2 GHz (f).

For a saturable absorber on a side-polished fiber the rotation of a polarization controller can switch laser generation between different pulse regimes [28]. Further, we demonstrate Q-switched regime and harmonic mode-lock (HML) generation obtained by proper polarization controller adjustment. It is important to discuss the effect of nonlinear polarization evolution (NPE) on the pulsed generation in our laser. First we remind, that SWCNT-SA provides 1.28 dB of PDL, which is well below the value of 2.7 dB required for NPE effect to contribute to the pulse shaping [7,36]. Second, we do not observe any signs of the NPE contribution like the shift of the emission line by the pump power increase or polarization controller rotation [37]. Thereby the NPE effect can be ruled out from the primary pulse

shaping mechanism in our mode-locked generation. We believe that the polarization controller rotation changes the linear and nonlinear loss amplitudes resulting in switching between different pulsating regimes [35].

By rotation of the polarization controller, we first find a Q-switched pulse generation shown in Fig. 7. The pulse parameters obtained from Fig. 7 for a 450 mW pump power are the following: the output power is 20 mW, Q-switched pulse duration measured from the pulse train is 1.27 μs, the pulse energy is 0.114 μJ, the spectral FWHM is 0.19 nm (Fig. 7(b)), and the repetition rate is 175 kHz.
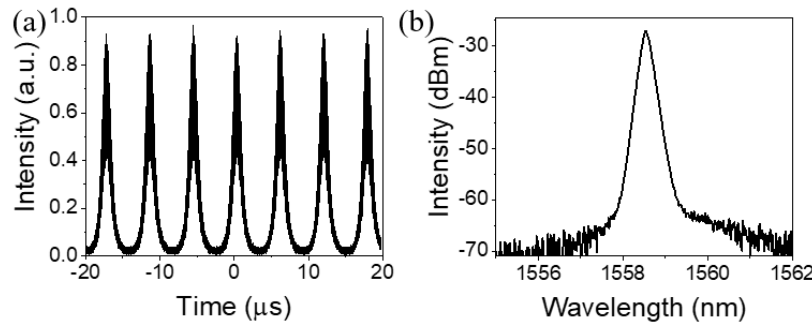

Fig. 7. Q-switched pulse generation: (a) the pulse train with the FWHM of 1.27μs and repetition rate of 175 kHz, (b) the pulse spectrum with the FWHM of 0.19 nm.

Next, we aim at the generation in HML regime. Following the strategy proposed in [38], by rotation of the polarization controller we find the soliton pulses with a minimal energy. This gives the highest HML order at the same pump power. For the current laser configuration, we find regime with a pulse energy of 5.3 pJ resulting in the 25th order (648.6 MHz repetition rate) of the harmonic mode-lock generation at 96.6 mW of pump power. Near the 26th and 27th harmonics the slope efficiency starts to decrease. In Fig. 8(a) pulse trains of the 1st, 5th, 16th and 27th HML orders are shown. The slope efficiency for the first 25 orders is 7.95 MHz/mW (see Fig. 8(b)).

Figure 8(c) shows pulse spectra of all HML orders, from the 1st to the 27th. We can see that the central wavelength does not change. Spectral FWHM increases from 1.1 to 2.8 nm with the HML order increase from the 1st to the 27th ones (see Fig. 8(d)). We note that the FWHM estimation for the first 3 orders may be not very accurate due to strong contribution of a continuous wave component. The measured spectral FWHM is about 3 times smaller compared to high energy pulse case which corresponds to longer pulse width (approximately 1.2 ps for transform limited pulses) in accordance with soliton area theorem [39].
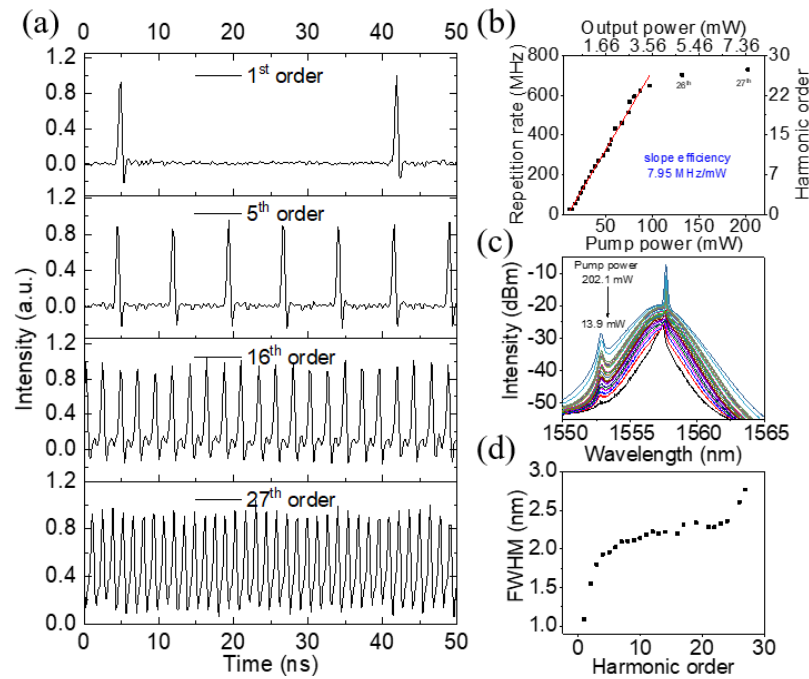
Fig. 8. Harmonic mode-lock pulse generation for lower orders: (a) pulse trains of the 1st, 5th, 16th and 27th orders. (b) Repetition rate, output power and harmonic order dependence from the pump power with calculated slope efficiency of 7.95 MHz/mW, (c) Optical spectra of HML pulses from the 1st to the 27th orders, (d) Spectral FWHM dependence on the harmonic order.

Finally, we use the same SWCNT-SA to obtain the harmonic mode-lock with higher pulse energy and harmonic order. For this purpose, we assemble a new laser with a longer resonator and higher negative net dispersion using 10 m length medium gain erbium-doped fiber with dispersion close to zero near the 1550 nm wavelength. The total cavity length is 20 m corresponding to the fundamental cavity repetition rate of 10.2 MHz with the net dispersion of -0.25 ps^2. For this scheme the number of the HML order is increasing stepwise with a pump power increase. The pulse energy is varying between 14.8 and 39 pJ. Typical sequence of the harmonic orders as a function of the pump is shown in Fig. 9(a). Here we obtain the 79th order as the highest one with the 895 MHz repetition rate and 31.5 mW output power at the pump power of 400 mW (Fig. 9(b)). The pulse energy is seven times higher reaching 39 pJ compared to short resonator laser. The spectral FWHM is 3.32 nm (see Fig. 9(c)) corresponding to slightly shorter pulse length compared to previous laser design. These pulse parameters are obtained at the cost of irregular harmonic order sequence. To address the laser generation stability, we measure the noise characteristic for the highest harmonic order and find supermode suppression ratio is equal to 40.4 dB (see Fig. 9(d)), which is sufficient for most of the applications.
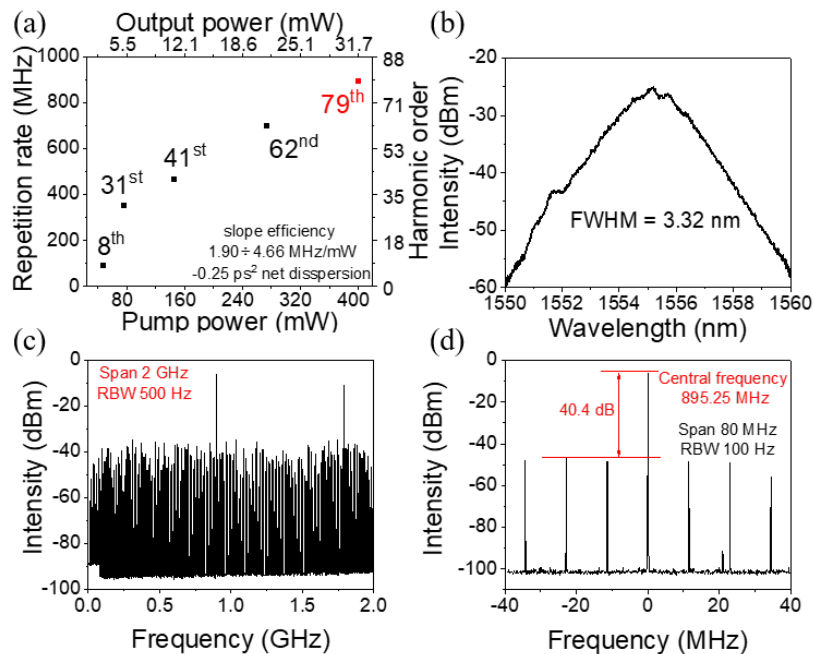
Fig. 9. Harmonic mode-lock pulse generation for higher orders: (a) Repetition rate, harmonic order, output power dependence on the pump power with the slope efficiency in the range of 1.90 ÷ 4.66 MHz/mW, (b) the 79th harmonic order optical spectrum with the FWHM of 3.32 nm, (c) radiofrequency spectrum for the 79th order of HML with 2 GHz span and (d) same with 80 MHz span and 100 Hz RBW.

In the end we address the thermal stability of the SWCNTs on a side-polished fiber. Earlier thermogravimetric studies demonstrated that the thermal stability of SWCNTs is governed by the oxidation process with critical temperature near 400 degrees [40,41]. To find the critical average power that our sample can withstand, we lunched a laser radiation into the sample and simultaneously determined the temperature of the SWCNTs above the fiber core by measuring the shift of the G-peak on the Raman spectra [42,43]. The setup scheme is shown on the Fig. 10(a). We pump the sample with two laser diodes (LD) at 980 nm connected to the sample by polarization combiner. Raman spectra is measured simultaneously with commercial Raman spectrometer Thermo Scientific DXRxi with 532 nm laser wavelength. Raman laser power was reduced to 0.6 mW so its effect on the SWCNT temperature was negligible. First, we measure the dependence of the G-peak position on the temperature without pump laser in the Linkam FTIR600 stage (allows heating up to 600 °C). G-peak shift coefficient is 0.025 cm^{-1}/K close to the measurements of other groups [42]. Next, we focus the Raman probe laser close to the front edge of SWCNT film where the pump power is at maximum and measured the temperature as a function of pump power. The results of the measurements are shown on Fig. 10(b) where dots represent the mean temperature and red cloud represents the error. We see that at maximum available power of 720 mW the temperature reaches 100 °C. The absorption of the sample at 980 nm is 1.1 times smaller compared to 1550 nm. Thus, the estimated laser power at 1550 nm needed to heat up the sample to the critical temperature of 400 °C is approximately 3 W. It is almost two orders of magnitude higher than the damage threshold for SWCNT-SA on connectors which does not exceed few tens of mW. Samples has also demonstrated good long-term stability:we were able to run the laser for more than a month and found no signs of the saturable absorber degradation.
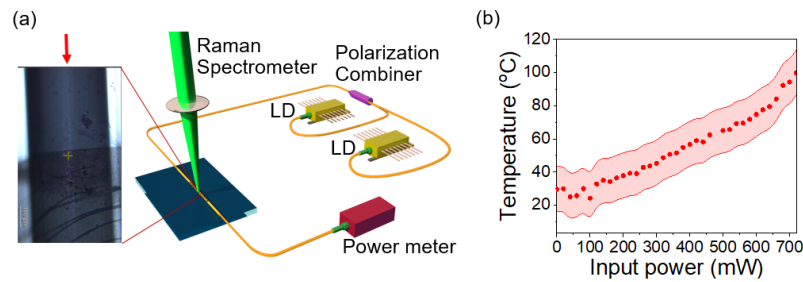
Fig. 10. (a) The experimental setup for the heating temperature measurement of the SWCNT-SA on the SPF. Inset shows photo of the SPF with SWCNTs in the Raman spectrometer microscope and a position of the laser spot. Red arrow indicates the direction of pump laser light propagation. (b) Temperature of the SWCNTs depending on the laser power through the SPF.

5. Conclusions

In conclusion, we have demonstrated the dry transfer technique for a polymer-free single-walled carbon nanotube saturable absorber fabrication on a side-polished fiber. Carbon nanotubes were synthesized by the aerosol floating catalyst method, collected on a cellulose filter and dry-transferred to a surface of the side-polished fiber. This method allows carbon nanotube saturable absorber fabrication in evanescent field interaction configuration in easy, robust and controllable way. The saturable absorber was fabricated with relatively low losses of 3.4 dB in nonpolarized light and possessed polarization depended losses of 1.3 dB to exclude nonlinear polarization evolution contribution to the pulse shaping. We demonstrated stable generation in mode-locked, harmonic mode-locked and Q-switched regimes in an erbium doped fiber laser. For a single pulse mode-locking we found regime with a 372 fs pulse width and 45 pJ pulse energy. For a harmonic mode-locking we detected the 62nd harmonic order of with a pulse energy equal to 30.2 pJ. We estimated the critical average power required to damage the sample and found it is close to 3 W. No signs of degradation of a saturable absorber was observed in the experiments during one month.

References

1. Q. Wang, T. Chen, B. Zhang, M. Li, Y. Lu, and K. P. Chen, "All-fiber passively mode-locked thulium-doped fiber ring laser using optically deposited graphene saturable absorbers," Appl. Phys. Lett. **102**(13), 131117 (2013).
2. B. Fu, Y. Hua, X. Xiao, H. Zhu, Z. Sun, and C. Yang, "Broadband Graphene Saturable Absorber for Pulsed Fiber Lasers at 1, 1.5, and 2 μm," IEEE J. Sel. Top. Quantum Electron. **20**(5), 411–415 (2014).
3. J. Sotor, G. Sobon, M. Kowalczyk, W. Macherzynski, P. Paletko, and K. M. Abramski, "Ultrafast thulium-doped fiber laser mode locked with black phosphorus," Opt. Lett. **40**(16), 3885–3888 (2015).
4. H. Yu, X. Zheng, K. Yin, X. Cheng, and T. Jiang, "Thulium/holmium-doped fiber laser passively mode locked by black phosphorus nanoplatelets-based saturable absorber," Appl. Opt. **54**(34), 10290–10294 (2015).
5. M. Jung, J. Lee, J. Koo, J. Park, Y.-W. Song, K. Lee, S. Lee, and J. H. Lee, "A femtosecond pulse fiber laser at 1935 nm using a bulk-structured Bi_2Te_3 topological insulator," Opt. Express **22**(7), 7865–7874 (2014).
6. Y. Cui, F. Lu, and X. Liu, "MoS_2-clad microfibre laser delivering conventional, dispersion-managed and dissipative solitons," Sci. Rep. **6**(1), 30524 (2016).
7. J. Koo, J. Park, J. Lee, Y. M. Jhon, and J. H. Lee, "Femtosecond harmonic mode-locking of a fiber laser at 3.27 GHz using a bulk-like, $MoSe_2$-based saturable absorber," Opt. Express **24**(10), 10575–10589 (2016).
8. S. Yamashita, Y. Saito, and J. H. Choi, *Carbon Nanotubes and Graphene for Photonic Applications* (Woodhead Publishing Limited, 2013).
9. S. Y. Set, H. Yaguchi, Y. Tanaka, and M. Jablonski, "Laser Mode Locking Using a Saturable Absorber

Incorporating Carbon Nanotubes," J. Lit. Technol. **22**(1), 51–56 (2004).

10. Z. Yu, Y. Wang, X. Zhang, X. Dong, J. Tian, and Y. Song, "A 66 fs highly stable single wall carbon nanotube mode locked fiber laser," Laser Phys. **24**(1), 015105 (2014).

11. D. Ma, Y. Cai, C. Zhou, W. Zong, L. Chen, and Z. Zhang, "37.4 fs pulse generation in an Er:fiber laser at a 225 MHz repetition rate," Opt. Lett. **35**(17), 2858–2860 (2010).

12. S. P. Su, Y. H. Xu, and C. A. Wilkie, "Thermal degradation of polymer-carbon nanotube composites," Polym. Nanotub. Compos. Prep. Prop. Appl. **2011**, 482–510 (2011).

13. S. Y. Ryu, K.-S. Kim, J. Kim, and S. Kim, "Degradation of optical properties of a film-type single-wall carbon nanotubes saturable absorber (SWNT-SA) with an Er-doped all-fiber laser," Opt. Express **20**(12), 12966–12974 (2012).

14. S. F. Bartolucci, K. E. Supan, J. M. Warrender, C. E. Davis, L. La Beaud, K. Knowles, and J. S. Wiggins, "Laser-induced thermo-oxidative degradation of carbon nanotube/polypropylene nanocomposites," Compos. Sci. Technol. **105**, 166–173 (2014).

15. A. Martinez and S. Yamashita, "Multi-gigahertz repetition rate passively modelocked fiber lasers using carbon nanotubes," Opt. Express **19**(7), 6155–6163 (2011).

16. A. Martinez and S. Yamashita, "10 GHz fundamental mode fiber laser using a graphene saturable absorber," Appl. Phys. Lett. **101**(4), 041118 (2012).

17. A. Martinez, K. Fuse, and S. Yamashita, "Enhanced stability of nitrogen-sealed carbon nanotube saturable absorbers under high-intensity irradiation," Opt. Express **21**(4), 4665–4670 (2013).

18. K. Kashiwagi, S. Yamashita, and S. Y. Set, "In-situ monitoring of optical deposition of carbon nanotubes onto fiber end," Opt. Express **17**(7), 5711–5715 (2009).

19. Y.-W. Song, S. Yamashita, E. Einarsson, and S. Maruyama, "All-fiber pulsed lasers passively mode locked by transferable vertically aligned carbon nanotube film," Opt. Lett. **32**(11), 1399–1401 (2007).

20. Y. W. Song, S. Yamashita, and S. Maruyama, "Single-walled carbon nanotubes for high-energy optical pulse formation," Appl. Phys. Lett. **92**(2), 021115 (2008).

21. A. G. Nasibulin, A. Kaskela, K. Mustonen, A. S. Anisimov, V. Ruiz, S. Kivistö, S. Rackauskas, M. Y. Timmermans, M. Pudas, B. Aitchison, M. Kauppinen, D. P. Brown, O. G. Okhotnikov, and E. I. Kauppinen, "Multifunctional free-standing single-walled carbon nanotube films," ACS Nano **5**(4), 3214–3221 (2011).

22. S. Kivistö, T. Hakulinen, A. Kaskela, B. Aitchison, D. P. Brown, A. G. Nasibulin, E. I. Kauppinen, A. Härkönen, and O. G. Okhotnikov, "Carbon nanotube films for ultrafast broadband technology," Opt. Express **17**(4), 2358–2363 (2009).

23. S. Kobtsev, A. Ivanenko, Y. G. Gladush, B. Nyushkov, A. Kokhanovskiy, A. S. Anisimov, and A. G. Nasibulin, "Ultrafast all-fibre laser mode-locked by polymer-free carbon nanotube film," Opt. Express **24**(25), 28768–28773 (2016).

24. A. Khegai, M. Melkumov, S. Firstov, K. Riumkin, Y. Gladush, A. Alyshev, A. Lobanov, V. Khopin, F. Afanasiev, A. G. Nasibulin, and E. Dianov, "Bismuth-doped fiber laser at 1.32 μm mode-locked by single-walled carbon nanotubes," Opt. Express **26**(18), 23911–23917 (2018).

25. H. Jeong, S. Y. Choi, F. Rotermund, Y.-H. Cha, D.-Y. Jeong, and D.-I. Yeom, "All-fiber mode-locked laser oscillator with pulse energy of 34 nJ using a single-walled carbon nanotube saturable absorber," Opt. Express **22**(19), 22667–22672 (2014).

26. Y.-W. Song, S. Yamashita, C. S. Goh, and S. Y. Set, "Carbon nanotube mode lockers with enhanced nonlinearity via evanescent field interaction in D-shaped fibers," Opt. Lett. **32**(2), 148–150 (2007).

27. H. H. Liu, K. K. Chow, S. Yamashita, and S. Y. Set, "Carbon-nanotube-based passively Q-switched fiber laser for high energy pulse generation," Opt. Laser Technol. **45**(1), 713–716 (2013).

28. J. Ko, H. Jeong, S. Y. Choi, F. Rotermund, D. Il Yeom, and B. Y. Kim, "Single-walled carbon nanotubes on side polished fiber as a universal saturable absorber for various laser output states," Curr. Appl. Phys. **17**(1), 37–40 (2017).

29. S. Y. Choi, H. Jeong, B. H. Hong, F. Rotermund, and D.-I. Yeom, "All-fiber dissipative soliton laser with 10.2 nJ pulse energy using an evanescent field interaction with graphene saturable absorber," Laser Phys. Lett. **11**(1), 015101 (2014).

30. J. Boguslawski, J. Sotor, G. Sobon, J. Tarka, J. Jagiello, W. Macherzynski, L. Lipinska, and K. M. Abramski, "Mode-locked Er-doped fiber laser based on liquid phase exfoliated Sb2Te3topological insulator," Laser Phys. **24**(10), 105111 (2014).

31. C. S. Jun, J. H. Im, S. H. Yoo, S. Y. Choi, F. Rotermund, D. I. Yeom, and B. Y. Kim, "Low noise GHz passive harmonic mode-locking of soliton fiber laser using evanescent wave interaction with carbon nanotubes," Opt. Express **19**(20), 19775–19780 (2011).

32. K. Mustonen, P. Laiho, A. Kaskela, T. Susi, A. G. Nasibulin, and E. I. Kauppinen, "Uncovering the ultimate performance of single-walled carbon nanotube films as transparent conductors," Appl. Phys. Lett. **107**(14), 143113 (2015).

33. A. G. Nasibulin, D. P. Brown, P. Queipo, D. Gonzalez, H. Jiang, and E. I. Kauppinen, "An essential role of CO2 and H2O during single-walled CNT synthesis from carbon monoxide," Chem. Phys. Lett. **417**(1–3), 179–184 (2006).

34. J. H. Im, S. Y. Choi, F. Rotermund, and D.-I. Yeom, "All-fiber Er-doped dissipative soliton laser based on evanescent field interaction with carbon nanotube saturable absorber," Opt. Express **18**(21), 22141–22146 (2010).

35. H. Jeong, S. Y. Choi, F. Rotermund, and D.-I. Yeom, "Pulse width shaping of passively mode-locked soliton fiber laser via polarization control in carbon nanotube saturable absorber," Opt. Express **21**(22), 27011–27016 (2013).

36. J. Bogusławski, G. Soboń, R. Zybała, K. Mars, A. Mikuła, K. M. Abramski, and J. Sotor, "Investigation on pulse shaping in fiber laser hybrid mode-locked by Sb$_2$Te$_3$ saturable absorber," Opt. Express **23**(22), 29014–29023 (2015).

37. K.-H. Lin, J.-J. Kang, H.-H. Wu, C.-K. Lee, and G.-R. Lin, "Manipulation of operation states by polarization control in an erbium-doped fiber laser with a hybrid saturable absorber," Opt. Express **17**(6), 4806–4814 (2009).

38. C. S. Jun, S. Y. Choi, F. Rotermund, B. Y. Kim, and D.-I. Yeom, "Toward higher-order passive harmonic mode-locking of a soliton fiber laser," Opt. Lett. **37**(11), 1862–1864 (2012).

39. D. S. Chernykh, A. A. Krylov, A. E. Levchenko, V. V. Grebenyukov, N. R. Arutunyan, A. S. Pozharov, E. D. Obraztsova, and E. M. Dianov, "Hybrid mode-locked erbium-doped all-fiber soliton laser with a distributed polarizer," Appl. Opt. **53**(29), 6654–6662 (2014).

40. V. Y. Iakovlev, Y. A. Sklyueva, F. S. Fedorov, D. P. Rupasov, V. A. Kondrashov, A. K. Grebenko, K. G. Mikheev, F. Z. Gilmutdinov, A. S. Anisimov, G. M. Mikheev, and A. G. Nasibulin, "Improvement of optoelectronic properties of single-walled carbon nanotube films by laser treatment," Diamond Related Materials **88**(May), 144–150 (2018).

41. A. Roch, T. Roch, E. R. Talens, B. Kaiser, A. Lasagni, E. Beyer, O. Jost, G. Cuniberti, and A. Leson, "Selective laser treatment and laser patterning of metallic and semiconducting nanotubes in single walled carbon nanotube films," Diamond Related Materials **45**, 70–75 (2014).

42. H. Fumin, Y. Kwok To, T. Pingheng, Z. Shu-Lin, S. Zujin, Z. Xihuang, and G. Zhennan, "Temperature dependence of the Raman spectra of carbon nanotubes," J. Appl. Phys. **84**(7), 4022–4024 (1998).

43. M. He, E. Rikkinen, Z. Zhu, Y. Tian, A. S. Anisimov, H. Jiang, A. G. Nasibulin, E. I. Kauppinen, M. Niemelä, and A. O. I. Krause, "Temperature dependent Raman spectra of carbon nanobuds," J. Phys. Chem. C **114**(32), 13540–13545 (2010).